The Journal of Chemical Physics

Diol it up: The influence of NaCl on methylglyoxal surface adsorption and hydration state at the air–water interface

Cite as: J. Chem. Phys. **153**, 164705 (2020); https://doi.org/10.1063/5.0017803
Submitted: 09 June 2020 • Accepted: 04 October 2020 • Published Online: 23 October 2020

Brittany P. Gordon, Grace A. Lindquist, Michael L. Crawford, et al.

The Journal of Chemical Physics ARTICLE scitation.org/journal/jcp

Diol it up: The influence of NaCl on methylglyoxal surface adsorption and hydration state at the air–water interface

Cite as: J. Chem. Phys. 153, 164705 (2020); doi: 10.1063/5.0017803
Submitted: 9 June 2020 • Accepted: 4 October 2020 •
Published Online: 23 October 2020

Brittany P. Gordon,[1,2] Grace A. Lindquist,[1] Michael L. Crawford,[1] Sumi N. Wren,[1,3] Frederick G. Moore,[4] Lawrence F. Scatena,[1] and Geraldine L. Richmond[1,a)]

AFFILIATIONS

[1] Department of Chemistry, University of Oregon, 1253 University of Oregon, Eugene, Oregon 97403, USA
[2] Department of Chemistry, University of California, Irvine, 1214 Natural Sciences II, Irvine, California 92697, USA
[3] Environment and Climate Change Canada (ECCC), Air Quality Research Division, 4905 Dufferin Street, Toronto, Ontario M3H 5T4, Canada
[4] Department of Physics, Whitman College, Walla Walla, Washington 99362, USA

Note: This paper is part of the JCP Special Collection in Honor of Women in Chemical Physics and Physical Chemistry.
[a)] **Author to whom correspondence should be addressed:** richmond@uoregon.edu

ABSTRACT

Methylglyoxal (MG)—an atmospherically important α-dicarbonyl implicated in aqueous-phase secondary organic aerosol formation—is known to be surface-active. Due to the presence of carbonyl moieties, MG can hydrate to form geminal diols in solution. Recently, it has been shown that MG exists predominantly as a monohydrate at the neat air–water interface. However, inorganic aerosol constituents have the potential to "salt-out" MG to the interface, shift its hydration equilibria, and catalyze self- and cross-oligomerization reactions. Here, we study the influence of the non-reactive salt, sodium chloride (NaCl), on the MG's surface adsorption and hydration state using vibrational sum frequency spectroscopy. The presence of NaCl is found to enhance MG's surface activity but not to the extent that water is fully excluded from the interface. Perturbations in the interfacial water structure are attributed to shifts in MG's hydration equilibrium at higher ionic strengths. Evidence of surface-active MG oligomer species is presented, but such oligomers are not thought to contribute significantly to the interfacial population. This work builds on the published studies on MG in pure water and gives insight into the interface's perturbation by NaCl, which has important implications for understanding MG's atmospheric fate.

I. INTRODUCTION

Secondary organic aerosols (SOA) have far-reaching effects on both the climate and human health. Aerosols influence the climate directly by scattering and absorbing light and indirectly by acting as nucleation sites in cloud formation.[1,2] Aerosol composition is complex and varied and consists of both inorganic and organic constituents.[3–6] Due to the high surface area to volume ratio of aerosols, molecules at aerosol surfaces play a particularly large role in their atmospheric chemistry.[7–9] Additionally, the presence of organics and salts can significantly affect SOA properties.[1–8,10] However, because of the complexity of SOA, much of how these components (individually or in concert) affect aerosol behavior remains unknown. This lack of knowledge makes predicting formation and aging of SOA in the atmosphere very challenging and currently a large source of errors in atmospheric modeling.

Methylglyoxal (MG) is an atmospherically important and abundant α-dicarbonyl, and the uptake and aqueous phase processing of MG has been shown to be an important source of SOA.[6,9,11–13] However, the chemistry underlying this SOA formation and subsequent aging is still uncertain due to the inherent complexity of MG, as it has multiple populated hydration states (a singly hydrated diol

and a doubly hydrated tetrol)[14,15] and also forms stable oligomer products with itself and other molecules.[5,13,16–18]

The unhydrated methylglyoxal monomer (MGM) hydrates preferably at the aldehydic carbon (α-C) to form methylglyoxal monohydrate [or methylglyoxal diol (MGD)] in aqueous solution. The monohydrate can subsequently be hydrated at the ketonic carbon (β-C) to form methylglyoxal dihydrate [or methylglyoxal tetrol (MGT)]. Both experimental studies[14] and thermodynamic calculations[19] suggest that methylglyoxal exists in a hydrated form in the bulk, with a MGD to MGT ratio of ~60:40 (Fig. 1). The hydration of MG has also been shown to be depth dependent. Wren *et al.*[15] demonstrated that this ratio is shifted at the air–water interface to favor the diol (~90% MGD to ~10% MGT). This is due to the less favorable solvation environment at the water surface and the lower surface affinity of MGT relative to MGD.

We have previously reported on the identification of pyruvic acid (PA) oligomer species at the aqueous interface.[20] Like PA, MG readily forms a large variety of oligomers, which include self-reactions with other MG as well as combining with other organics and reactive-salts.[5,13,16–18,21] In fact, De Haan *et al.* reported that in aqueous MG solutions, only 53% of the actual molecular species were monomeric MG.[13] Of the remaining constituents, the MG dimer and oligomer products were found to account for 37%, while PA and hydroxyacetone (HA) each accounted for ~5%.[13]

However, those experiments were performed in neat water, which is not representative of the high ionic strength found in atmospheric particulates.[1–8,22] Alone, atmospheric salts can affect the water structure at the air–water interface (i.e., the aerosol surface), thereby altering aerosol hygroscopicity and surface tension (ST).[3–5] The presence of salts, and corresponding change in the activity of water, can also shift the hydration equilibrium of organics with multiple hydration states.[16,23] Salts also have the potential to influence the uptake of MG and other organics to the condensed phase (via "salting-in" and "salting-out" effects), as well as to catalyze and participate in oligomerization reactions leading to SOA formation.[3,6,24] Here, "salting-out" refers to enhanced bulk to surface partitioning of the organics component to the interface. Conversely, "salting-in" refers to instances where salt increases the solubility of a molecule, which can increase the uptake of organics to aerosol from the gas phase.[3,6,22,24–26]

Considering the multiple favorable hydration and oligomer species that form spontaneously in MG solutions, it is clear that this system cannot be treated as a single organic and instead should be viewed as a mixed system. This distinction is important as an aerosol with multiple organic species can have unpredicted synergistic effects on aerosol surface tension and hygroscopicity, particularly in the presence of salt.[6,27] These effects have been ascribed to the adsorption of mixed organics to the particle interface that exceed what would be expected based on the predictions from bulk properties.[6,27] Changes in these properties can have important atmospheric consequences, such as enhancing aerosol cloud nucleation activity.[1–3,5,6,22,24–26]

In this study, the influence of the non-reactive salt NaCl on MG's surface behavior at the air–water interface is examined using vibrational sum frequency (VSF) spectroscopy and surface tensiometry. A combination of computational density functional theory (DFT) and molecular dynamics (MD) are employed to further decouple and understand the interfacial species of this system. The results indicate that NaCl further shifts the hydration equilibrium of MG to favor the diol as the predominant species at the interface, with lesser amounts of MGT. However, MGD is not alone at the interface and is joined by what is likely a multitude of oligomeric species in lower concentrations. This work has implications for understanding the atmospheric fate of methylglyoxal and other important α-dicarbonyls.

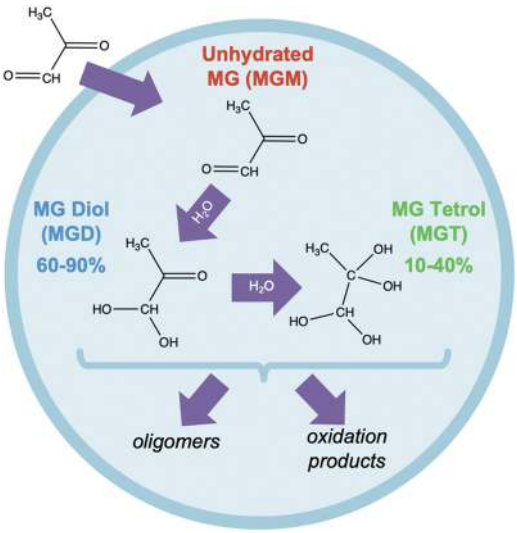

FIG. 1. In-cloud aqueous phase processing[14,15] of unhydrated (MGM), singly hydrated (MGD), and doubly hydrated (MGT) methylglyoxal.

II. METHODS

A. Vibrational sum frequency (VSF) spectroscopy theory

Vibrational sum frequency (VSF) spectroscopy is a surface selective technique ideally suited to the study of molecules at interfaces. VSF spectroscopy is a well-established technique,[15,28–63] and only a brief description is provided here. A fixed-frequency visible beam is overlapped spatially and temporally with a tunable infrared (IR) beam at an aqueous surface, producing a third beam at the sum of the two incident frequencies (the sum frequency beam). When the IR field is coincident with a vibrational mode that is both IR and Raman active, there is a resonant enhancement in the intensity of the sum frequency (SF) beam. Selection rules additionally require that the vibrational mode resides in a region of broken symmetry; hence, molecules residing in an asymmetric environment (such as that present at an interface) give rise to a SF response, while those residing in a symmetric environment (the isotropic bulk) do not.

The intensity of the generated SF signal is proportional to the square modulus of the second-order susceptibility, $\chi^{(2)}$, which has both resonant and nonresonant components. The resonant component is proportional to the number of contributing molecules,

N, and the orientational average of the molecular hyperpolarizability, β. Therefore, VSF spectra contain information about surface population and orientation.

VSF spectroscopy is a coherence technique leading to the constructive and destructive interference of overlapping modes. A standard fitting routine is used to deconvolve the nonresonant signal and the individual resonant modes according to the following equation:[28]

$$\chi^{(2)} = \chi^{(2)}_{NR} e^{i\psi} + \sum_v \int_{-\infty}^{\infty} \frac{A_v e^{i\varphi_v} e^{-\left[\omega_L - \omega_v / \Gamma_v^2\right]^2}}{\omega_L - \omega_{IR} + i\Gamma_L} d\omega_L. \quad (1)$$

The first term is the nonresonant second-order susceptibility and is described by an amplitude and a phase, ψ. The second term describes the resonant contribution and is a sum over the individual resonant vibrational modes. The line shape of each mode is fit as a convolution of empirical homogeneous, Γ_L, and inhomogeneous broadening, Γ_v. The amplitude, A_v, describes the transition strength and contains the product of the number of contributing molecules and the IR and Raman transition probabilities. The frequencies of the Lorentzian, IR, and resonant vibrational mode are given by ω_L, ω_{IR}, and ω_v, respectively. The phase of each resonant mode is given by φ_v and is either 0 or π. In this work, Lorentzians of 2 cm^{-1}, 5 cm^{-1}, and 12 cm^{-1} were used to describe the CH, both the coordinated OH and C=O, and the "free OH" vibrational modes, respectively.[64–67]

B. Laser system

VSF spectra were obtained using a picosecond sum frequency system that has been fully described elsewhere.[20,42] Briefly, a mode-locked Ti:sapphire system in tandem with an ultrafast regenerative amplifier is used to produce a pulsed visible beam centered at 800 nm. A portion of the visible beam is sent through an optical parametric amplifier (OPA) in tandem with a difference frequency generator (DFG) to produce a tunable IR beam (2.5 μm–12 μm). The visible and IR beams are copropagated to the interface at 63° and 55° from the surface normal, respectively. The resulting sum frequency beam is detected using a thermoelectrically cooled CCD camera. Samples are held in scrupulously clean, shallow glass dishes on a translatable stage.

C. Spectral analysis

VSF spectra were acquired by measuring the intensity of the SF beam as the tunable IR beam was scanned in 3 cm^{-1} increments over the relevant spectral range (~2700 cm^{-1} to 3850 cm^{-1} for the CH/OH stretching region and ~1500 cm^{-1} to 1850 cm^{-1} for the C=C/C=O stretching region). Spectra were acquired in the *ssp* and *sps* polarization schemes where the three letters denote the polarizations of the sum frequency, visible, and IR beams, respectively. The different polarization schemes allow different molecular orientations to be probed with *ssp* and *sps* probing molecular dipole components perpendicular and parallel to the interface, respectively. All spectra presented here have been normalized to the nonresonant response from an uncoated gold surface. IR wavelengths were calibrated daily against a polystyrene standard. The presented spectra are averages from >3 scans. All measurements were performed at ambient temperature (~20 °C).

D. Surface tension measurements

Surface tension (ST) measurements were performed using the Wilhelmy plate method. Solutions were placed in a clean glass dish, and a Pt plate was lowered to the air–water interface. A force balance (KSV Instruments) measuring the force acting on the Pt plate was used to obtain surface tension (mN/m) data as a function of time (s). The Pt plate was rinsed with nanopure water and cleaned under flame between measurements.

The ST of water (~72.8 ± 0.5 mN/m) and 1M NaCl (~74.3 ± 0.5 mN/m) were measured daily for reference. Surface tensions were converted to surface pressures (SP) by subtracting the daily-measured surface tension of the relevant reference solution (i.e., water for the neat-MG and 1M NaCl for NaCl–MG solutions).

It is worth noting that 1M NaCl is considerably lower than the ionic strength generally observed in the atmospheric aerosol, which regularly exceeds 3M.[22,69,70] This idealized concentration was chosen here to minimize laser scattering and precipitation into the platinum plate in VSF and ST experiments, respectively.

E. Sample preparation

Aqueous MG solutions were prepared volumetrically by diluting an aqueous stock MG solution (40 wt. %, Sigma Aldrich) in nanopure (18.2 MΩ cm) water. The NaCl salt (ACS grade >99.0%, EMD Chemicals) was baked at 220 °C for at least 48 h before use to eliminate organic contaminants. Solutions were prepared ≥24 h before use and stored in Pyrex glass flasks. Solutions were not further protected since photochemical degradation was not a concern.[3]

To confirm that the stock MG hydration matched that reported in the literature, ^{1}H and ^{13}C NMR, 2D HSQC (heteronuclear single quantum correlation), and ^{15}N NMR (Figs. S5–S7 of the supplementary material) were performed on solutions of MG. The results showed that the bulk MGD:MGT ratio was ~60%–65% to 35%–40%, in agreement with the literature.[14,19,68] Since the N—H bending modes of primary amines occur in the 1650 cm^{-1}–1580 cm^{-1} region, ^{15}N NMR was performed as well (Fig. S8), which confirmed that no nitrogen contamination is present.

F. Computational methods

Molecular dynamics (MD) simulations are performed using the Amber 12[71] suite of programs from starting configurations generated by PACKMOL.[72] Parameters and force fields are derived in the same manner described in previous studies.[15,35–42] Simulations of pure systems refer to those previously reported for neat-MG and were not repeated here. Classical molecular dynamics (MD) simulations were performed for the systems of isolated nonreactive MG hydration species and 1M NaCl. In each simulation, 16 MG, 16 NaCl, and 900 water molecules are arranged to form a 30 Å cube within a 30 × 120 × 30 $Å^3$ simulation box (corresponding to ~1M organic and salt concentrations) with periodic boundary conditions, creating a water slab with two interfaces. These simulations are energy minimized at 0 K and then equilibrated from 0 K to 298 K over 2 ns followed by subsequent evolution at 298 K for 50 ns in 1 fs time steps.

The results of these simulations were combined with quantum mechanical density functional theory (DFT) conformer libraries created for the previously reported neat-MG[15] using the Gaussian 09[73] program package at the B3LYP/6-311++G(2*d*, 2*p*) level of theory. These DFT libraries include energy optimized stationary point structures, harmonic frequencies, and anharmonic correction, as well as polarizabilities and dipole moment derivatives calculated using three-point finite differentiation. MD trajectories are analyzed at every time step to match molecule conformations within the library of gas-phase DFT structures using an in-house code.[35] Density profiles and bond angle orientations are determined for each MG hydration species.

To generate VSF intensities and phases, the code combines the MD and DFT results to approximate the second-order nonlinear susceptibility response tensor for each normal mode of a given MG conformer according to the following equation:

$$\chi^{(2)}_{ijk} \propto \sum_{a,b,c} C_{abc} \frac{\partial \alpha_{ab}}{\partial Q_q} \frac{\partial \mu_c}{\partial Q_q}. \quad (2)$$

In Eq. (2), α is the molecular polarizability, μ is the dipole moment, Q_q is the normal coordinate of the mode q, and C is a geometrical factor relating the molecular and laboratory reference frames.

The results from simulations of mixed MGD and MGT were not found to differ appreciably from simulations of "pure" hydration species. As such, this discussion will include only the results of the pure simulations of 16 molecules (~1M organic concentration) of MGM, MGD, or MGT (only one type of hydration species per simulation).

III. EXPERIMENTAL RESULTS AND DISCUSSION

A. Surface activity

Surface pressure (SP) isotherms at constant NaCl concentration (0M and 1M) and varying MG concentration are shown in Fig. 2(a). Methylglyoxal in neat water has previously[3,15] been shown to be strongly surface-active, with a maximum SP > 15 mN/m. The addition of 1M NaCl further increases this surface activity by ~4 mN/m to 6 mN/m on average.

Sareen *et al.*[3] also measured the surface tension of mixed NaCl–MG systems and found that the presence of NaCl enhances MG's surface activity (up to 10 mN/m for 5.1M salt). They attribute the enhanced surface activity to a salting-out influence of NaCl. However, it is important to note that the salting-out effect of NaCl is significantly less than other salts.[3,22] Indeed, the overall increase in SP with the addition of salt is somewhat minimal when viewed in the context of the SP isotherm of other similar organics.

The SP isotherms of pyruvic acid (PA)[20] and hydroxyacetone (HA)[42] are also displayed in Fig. 2(a). Similar to MG, PA is a dicarboxylic acid with two favorable hydration states [unhydrated PA and a hydrated PA triol, Fig. 2(b), top] as well as a multitude of oligomer products such as zymonic acid (ZYA) and parapyruvic acid.[20,23,74–86] Conversely, HA is an α-hydroxyketone that is known to exist 96%–98% in its unhydrated monomeric form in aqueous solutions [Fig. 2(b), bottom].[42,87] HA is very similar in structure to the MG diol, differing only in having a second hydrogen atom in place of one of the MGD's geminal diols.

Even with the addition of salt, the SP values of MG are significantly lower than those of PA for the same concentration, while HA is definitively lower than neat-MG. This is interesting given that the more polar PA, particularly in its triol form, would ostensibly be more soluble than MG while HA, being slightly more hydrophobic with its additional CH, would be expected to be more surface-active than HA. However, this is clearly not the case.

Given that MG and PA share the preference to hydrate and form oligomers, while HA does not, it seems likely that these additional products are contributing to the measured surface pressures. In fact, Gordon *et al.* recently published work demonstrating the presence of surface-active PA oligomers at the air–water interface.[20] It is also worth noting that VSF studies of both PA and HA show ordered water at the interface at 1M.[20,42] PA, in particular, demonstrates that water remains at the interface at higher SP than those seen for MG–NaCl.[20] Thus, it is unlikely that the ~3 mN/m to 5 mN/m increase upon the addition of NaCl is enough to exclude water from the interface in MG solutions. Overall, it

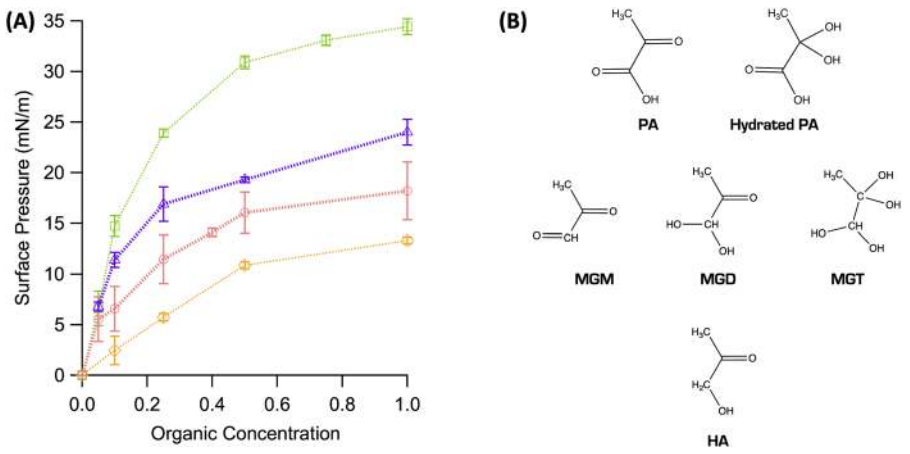

FIG. 2. Surface pressure isotherm vs organic concentration for MG and MG–NaCl: (a) Surface pressure as a function of bulk methylglyoxal concentration for aqueous solutions with 0M NaCl (pink circles, from Wren *et al.*, 2015[15]) and 1M NaCl (purple triangles). SP isotherms of hydroxyacetone (orange diamonds)[42] and pyruvic acid (green squares)[20] are provided for context. (b) Structures of PA, MG, and HA.

becomes clear that while salt definitely increases surface partitioning in MG solutions, other factors are at play as well.

B. VSF spectroscopy results

We have previously reported on MG's surface behavior at the air–water interface.[15] However, since that time a significant number of improvements to the picosecond laser system have resulted in much-increased signal to noise, yielding superior data and revealing spectral features previously buried in, or nearly in, the noise level. This has allowed for a more in-depth analysis than was previously available. As such, updated spectra (Fig. 3) and fitting assignments (Table I) of the MG–neat water system are included in this discussion.

VSF spectra were acquired in the *ssp* and *sps* polarizations of the C=C/C=O [Figs. 3(a) and 3(d)], C–H [Figs. 3(b) and 3(e)], and O–H [Figs. 3(c) and 3(f)] stretching regions for neat water and 1M MG with 0.1M and 1M NaCl. A brief discussion on the VSF spectra of neat water is provided in the supplementary material. Each spectral region contains strong VSF responses arising from MG, and dramatic changes are observed upon the addition of NaCl.

In brief, at the neat air–water interface, strong contributions from MG are visible in the C=O, CH, and OH stretching regions. A notable feature in the neat-MG spectrum is the enhancement of coordinated OH stretching modes between 3100 cm^{-1} and 3600 cm^{-1}. The addition of salt appears to suppress this coordination while also the intensity of the lower frequency CH stretching modes increases. While the reasons for these changes may initially seem straightforward, such as increased surface partitioning, a careful examination of the results reveals a more interesting picture.

1. CH stretching region

As previously reported, MGD and MGT have distinctive spectral contributions in the CH stretching region, which is demonstrated in Fig. 4 by comparison of the experimental spectra [Figs. 4(a) and 4(c)] to the calculated sum frequency responses [Figs. 4(b) and 4(d)]. The calculated VSF intensities and phases (herein referred to as "stick spectra") of each individual mode of each conformer MGM, MGD, and MGT are color coded to their respective structure in Fig. 3(e), with positive intensities indicating positive phases and vice versa. These stick spectra provide insight into how individual contributions give rise to the overall spectrum and were used in combination with the calculated density profiles to determine that the diol to tetrol ratio is greater at the interface than in the bulk, favoring the diol (40% MGD to 60% MGT in the bulk[14] vs 90% MGD to 10% MGT at the interface.[15]

For the neat-MG system, two broad features dominate the CH stretching region [Figs. 4(a) and 4(c)]. In both polarizations, a broad lower frequency peak between 2860 cm^{-1} and 2870 cm^{-1} is attributed primarily to the α-CH stretching mode of MGD (blue). The higher frequency peak is centered at ~2935 cm^{-1} and ~2975 cm^{-1} for the *ssp* and *sps* polarizations, respectively, and contains contributions from both the symmetric methyl stretching mode of MGD (blue) and the α-CH stretching mode of MGT (MGT). Another important feature in the *ssp* polarization spectrum is the lower intensity shoulder centered at ~2980 cm^{-1}, which has previously been found to primarily arise from the symmetric methyl stretching mode of MGT. Similarly, the *sps* polarization spectrum also exhibits a shoulder on the high energy side of the region. This shoulder is centered at ~3000 cm^{-1} and contains responses from the asymmetric methyl stretching modes of both MGD and MGT.

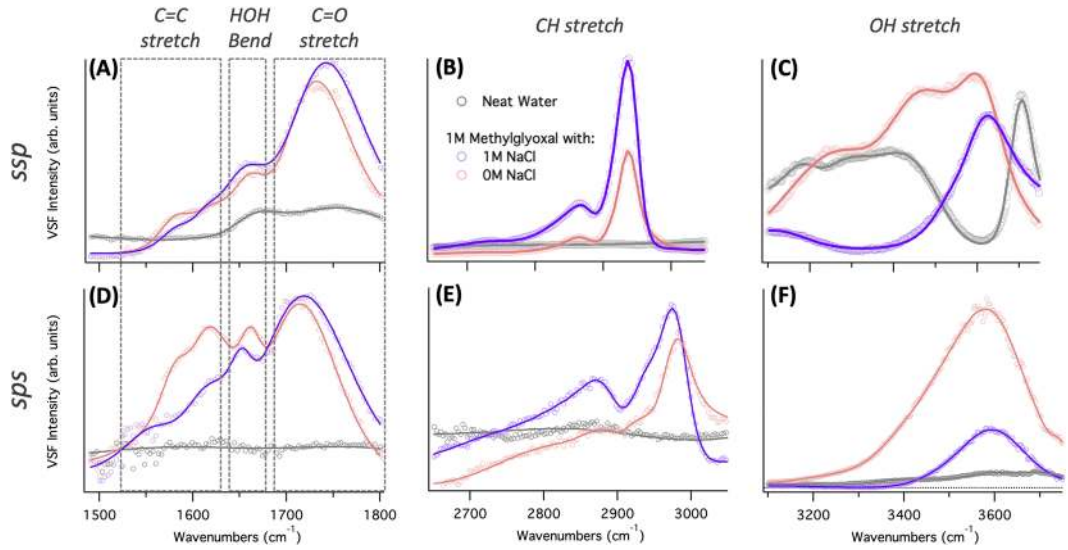

FIG. 3. VSF experimental spectra for MG and MG–NaCl in H_2O: VSF experimental data (open circles) and corresponding fits (solid lines) for water and aqueous MG and MG–NaCl in the *ssp* [(a)–(c)] and *sps* [(d)–(f)] polarization schemes for the C=C/C=O stretching region (left), the CH stretching region (middle), and the OH stretching region (right). Water (gray), 1M MG (pink) and 1M MG with 1M NaCl (purple). Dotted boxes [(a) and (d)] provide the visual reference of approximate spectral regions.

TABLE I. Fit assignments for MG–NaCl: frequencies (cm^{-1}) and assignments for peaks contributing intensity to experimental and calculated *sps* spectra. Reported experimental frequencies obtained from global fitting of the experimental spectra. Experimental uncertainty = ±18 cm^{-1}.

ssp Expt. Freq.	Calc. Freq.	Assignment (mode, species)	*sps* Expt. Freq.	Calc. Freq.	Assignment (mode, species)
~1575	. . .	C=C MG oligomer	~1621	. . .	C=C MG oligomer
~1660	. . .	HOH bend	~1660	. . .	HOH bend
1742	1738 1751 1752 1768 1781	α-C=O, MGM1 β-C=O, MGD1 β-C=O, MGD3 β-C=O, MGM1 β-C=O, MGD2	1718	1738 1751 1752 1768 1781	α-C=O, MGM1 β-C=O, MGD1 β-C=O, MGD3 β-C=O, MGM1 β-C=O, MGD2
~2750	2777	α-CH, MGM1 COOH dimers	~2775	2777	α-CH, MGM1 COOH dimers
2878	2834 2860 2870	α-CH, MGT3 α-CH, MGD2 α-CH, MGD3	2878	2834 2860 2870	α-CH, MGT3 α-CH, MGD2 α-CH, MGD3
2940	2929 2932 2938 2941	CH_3-SS, MGD2 CH_3-SS, MGD1 CH_3-SS, MGD2 α-CH, MGT2	2940	2940 2942	CH_3-AS, MGD2 CH_3-AS, MGM1
2972	2970 2981	CH_3-SS, MGT2 CH_3-SS, MGT3	2988	2969 2973 2998 2997 3000 3000	CH_3-AS, MGT2 CH_3-AS, MGT3 CH_3AS', MGM1 CH_3-AS', MGD3 CH_3-AS', MGD1 CH_3-AS', MGD2
3540, 3544	3460 3633 3646 3667	MG-OH, MGD3 MG-OH, MGD3 MG-OH, MGD1 MG-OH, MGD2	3517, 3538	3633 3647 3667	MG-OH, MGD3 MG-OH, MGD1 MG-OH, MGD2

The addition of salt creates distinct intensity changes in the CH stretching region, but analysis reveals no appreciable shift in the frequency position. In both polarizations, the two dominant spectral features dramatically increase in intensity with increasing salt but the intensity of the high frequency shoulders also sharply decreases. The spectral fitting indicates that the intensity changes observed in the coordinated OH region (discussed further below) do not affect the CH stretching fit intensities and thus do not account for this behavior. As these intensity changes are consistent between polarizations, they cannot be explained by reorientation. Likewise, the intensity does not uniformly increase and so cannot be entirely justified by increased surface population, either.

As previously stated and demonstrated in Figs. 4(b) and 4(d), the lower frequency feature at 2870 cm^{-1} arises primarily from MGD, while the majority of MGT contributions occur above 2940 cm^{-1}. This suggests that for the MG–NaCl system, there is an overall increase in intensity for modes associated with MGD (and potentially MGM). Conversely, modes associated with MGT decreased in intensity, indicating that these changes are related to MG's hydration equilibrium.

It is worth noting that in both polarizations, a broad low intensity region centered around ~2725 cm^{-1} extends to the low frequency side of the spectrum and also increases with added NaCl. This intensity could be arising from two potential sources: (1) the aldehydic CH stretching mode of MGM[15] and/or (2) OH stretching modes from hydrogen bonded carboxylic acid dimers of MG oligomer products.[74] Option 1 would be consistent with a shift in the MG equilibrium toward its less hydrated forms, while option 2 could indicate an increase in MG oligomer formation, which has been observed with the loss of water in drying studies of MG. While the source of this mode cannot be resolved here, either of these options indicates noteworthy chemistry occurring at the interface.

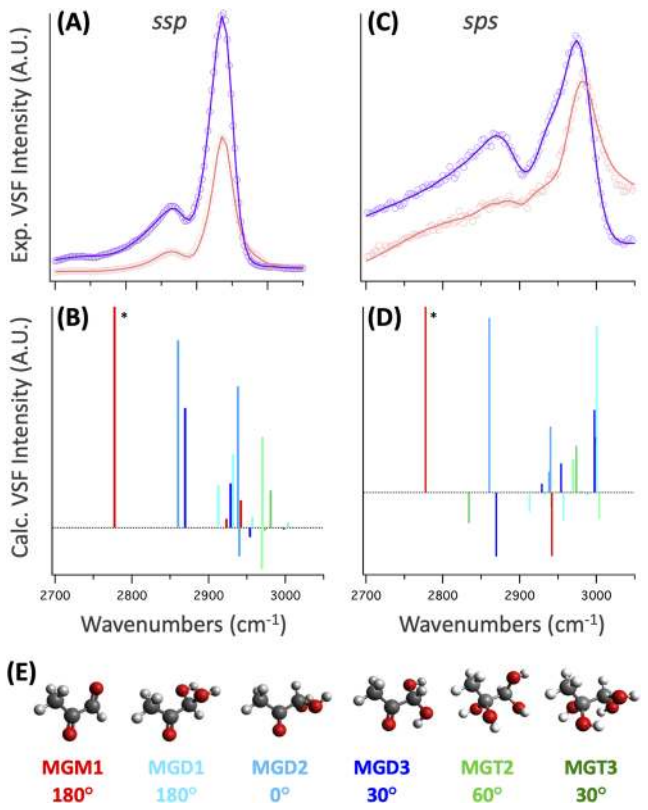

FIG. 4. Experimental VSF MG and MG–NaCl vs calculated VSF stick spectra: experimental vs calculated VSF spectra from MG species simulation in CH stretching regions. *ssp* (a) and *sps* (c) experimental VSF spectra of 1M MG (pink) and 1M MG with 1M NaCl (purple). Calculated intensities and phases for the individual conformer contributions in the *ssp* (b) and *sps* (d) polarizations for each MG conformer, color coded to their respective structures in (e), where positive and negative intensities represent the phases of zero and pi, respectively. (e) Gas phase DFT structures of each MG conformer at the B3LYP/6-311++G (2*d*, 2*p*) level of theory.

2. C=C/C=O stretching and HOH bending region

The region from ~1500 cm^{-1} to 1800 cm^{-1} has a high degree of spectral density, containing modes from MG C=O stretching, water bending, and (as will be demonstrated below) C=C stretching modes from MG oligomers.

Based on the evidence in the CH stretching of a further hydration shift, it is important to determine if water is still contributing to the interface. While intensity in the coordinated OH stretching region is largely suppressed in the MG–NaCl system, it is possible that less coordinated water is contributing to the peak at ~3650 cm^{-1}. While such contributions cannot be experimentally decoupled from those of the MG-OH stretching modes of MGD and MGT, the bending modes of water are spectrally distinct from those of MG. Indeed, for both the *sps* and *ssp* polarizations [Figs. 3(a) and 3(d)], a contribution at ~1660 cm^{-1} is present for both neat MG and NaCl solutions. This region is coincident with the bending mode of water (Fig. S1), which has previously been observed for PA[42] and HA,[20] and is thus attributed to ordered interfacial water here.

Figure 5(a) shows the *ssp* C=C/C=O stretching region of water, neat 1M MG, and 1M MG with 1M NaCl. In Fig. 5 (and offset for clarity) are 1M HA and 1M PA (green) solvated in H_2O (circles) and D_2O (triangles). While the water bending mode is less clear in PA, its absence can be seen in decreased intensity in the C=O stretching region when solvated in D_2O. From this, it considered likely that water also contributes some intensity to the C=O stretching mode of both neat-MG and with NaCl.

Notably, the frequency position of the *sps* C=O stretching modes [Fig. 3(d)] was fit to 1718 cm^{-1}, which is over 20 cm^{-1} lower than the *ssp* frequency position [Fig. 3(a)] at 1742 cm^{-1}. Due to the extensive spectral congestion in this region, the source of this frequency shift cannot be determined here. However, such a shift could suggest that C=O stretching components parallel to the interface (*sps*) tend to be more hydrogen bonded than the perpendicular (*ssp*) counterparts. Alternatively, it could be indicative of multiple C=O stretching peaks with differing *sps* and *ssp* favorability, as was observed with HA.[42]

This region also contains broad features that were fit to ~1575 cm^{-1} in the *ssp* polarization and ~1620 cm^{-1} in the *sps* polarization. Comparison to PA once again lends insight, as a similar feature at ~1630 cm^{-1} was found to arise from surface-active PA oligomers including zymonic acid (ZYA). Numerous studies have established the production and mechanistic pathways of MG oligomers that contain C=C moieties.[5,13,21] While it is not possible to identify the specific oligomer from this alone, we are confident in attributing this feature to general C=C stretching modes of MG oligomers.

Interestingly, the intensity of these peaks decreases in both polarizations with the addition of salt. As the decrease in intensity in one polarization does not correspond to the increase in the other,

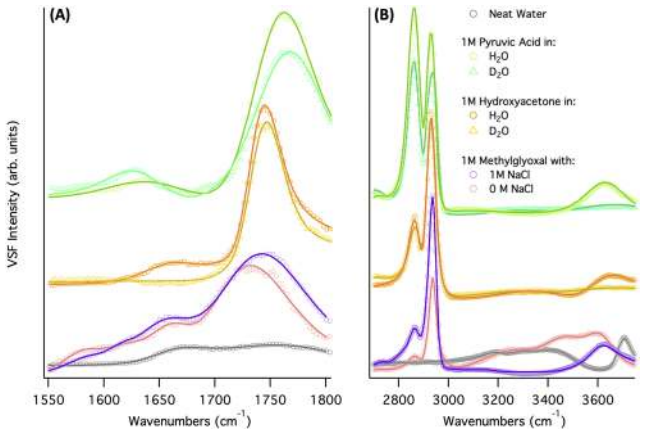

FIG. 5. VSF spectra for MG and MG–NaCl vs HA and PA in H_2O and D_2O: VSF experimental *ssp* spectra in H_2O (open circles) and D_2O (open triangles) with the corresponding fits (solid lines) in the (a) C=C/C=O and (b) CH/OH stretching regions for: (bottom) 1M MG and 1M MG (pink) with 1M NaCl (purple), (middle) offset 1M HA in H_2O[42] (yellow) and 1M HA in D_2O[42] (orange), and (top) offset 1M PA in H_2O[20] (dark green) and 1M PA in D_2O (light green).

this loss is unlikely to be due to reorientation alone. An intriguing possibility is that the higher ionic strength drives the oligomerization equilibrium away from these species. However, further work would need to be done to better understand the mechanisms producing such species as well as how they may be affected by non-reactive salts.

This suggestion of oligomers is compelling, but unlike PA, there are no other clear indications of oligomeric species at the interface as the CH stretching modes of MG's hydration species can account for all features observed in that region. Additionally, the C=C mode observed here is significantly broader than that in PA. Likely, this means that there is a larger assortment of oligomeric species populated. Thus, instead of yielding strong and relatively sharp resonances, MG oligomers contribute to a continuum of modes that serve to further broaden and obscure the spectra. Likewise, any MG oligomer species present that share similar resonance frequencies to those of the monomeric MG will contribute to the overall spectral broadening and congestion in their respective regions. Although fully exploring the oligomeric products of MG is beyond the scope of this work, insight can be gained by computationally examining the MG hydration equilibrium.

3. OH stretching region

In both polarizations, the OH stretching region of neat MG is substantially enhanced above that of neat water. This was previously observed for MG, but a definitive cause could not be identified.

In the more distinctive *ssp* spectra, much of the characteristic spectral shape and underlying frequencies of coordinated OH modes are preserved in the enhanced MG OH stretching spectra. Additionally, this region's intensity is not extended to lower frequencies, as is generally seen when the response of coordinated OH modes is enhanced due to the field effects from charged species. However, here, it can be seen that this enhancement diminishes with increasing salt concentration, as shown in Fig. 6, providing us insight into this previously enigmatic observation.

Figure 5(b) shows the CH/OH stretching region of water, neat 1M MG, and 1M MG with 1M NaCl compared to offset 1M HA (orange) and 1M PA (green) solvated in H_2O (circles) vs D_2O (triangles). Looking at the OH stretching region of both HA and PA, it is clear that the enhancement observed with neat-MG and low ionic strength MG–NaCl is not the norm for these systems. Again, this suggests that the loss of coordinated OH intensity with increasing salt is actually a return to the conventional line shape for these kinds of molecules.

Given this as well as the changes observed in the CH stretching region provides a potential explanation: the salt, as well as the increased overall MG surface presence from salting out effects, has decreased the total amount of water at the interface available for hydration, making it less favorable to hydrate MGD to form MGT. As MGT has four OH groups, it has the ability to enhance the ordered hydrogen bonding beyond that of any of the other MG or PA hydration species of MG and PA or of HA. As the hydration equilibrium shifts with increasing NaCl to further favor MGD, this heightened H-bonding decreases until the coordinated OH stretching returns to the more expected line shape at ~0.1M NaCl and above.

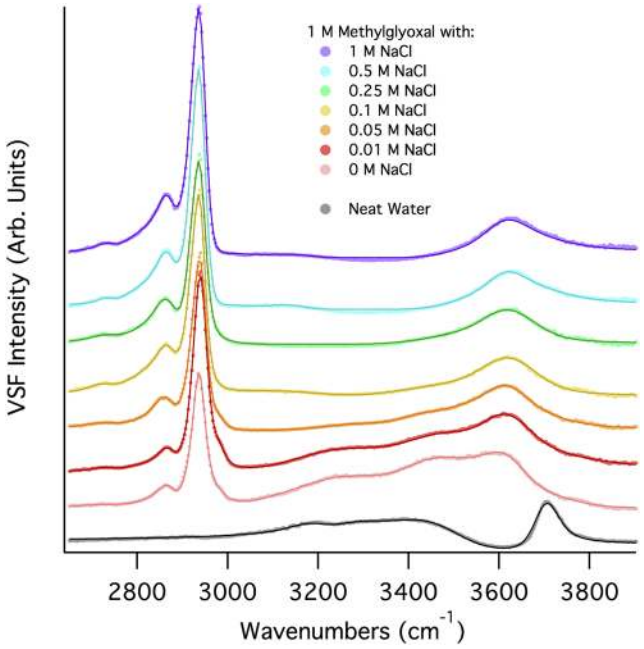

FIG. 6. VSF spectra of MG and MG–NaCl CH/OH stretching regions: Offset VSF experimental data (open circles) and corresponding fits (solid lines) for water (gray) and aqueous 1M MG solutions with increasing NaCl concentration in the *ssp* CH/OH stretching region. Offset traces correspond to 1M MG with 0M NaCl (pink), 0.01M NaCl (red), 0.05M NaCl (orange), 0.1M NaCl (yellow), 0.25M NaCl (green), 0.5M NaCl (blue), and 1M NaCl (purple).

Thus, we conclude that the presence of salt, as well as the increased overall MG surface presence from salting out effects, has decreased the total amount/activity of water at the interface available for hydration, making it less favorable to hydrate MGD an additional time to form MGT.

IV. CALCULATED RESULTS

A. Calculated density profiles

To further explore this complex system, MD simulations were examined to determine the depth dependent partitioning and orientation of each MG species. The profiles depicted in Fig. 7(a) provide information about the density of each MG hydration state (mol/l, left) as well as that of water (g/ml, right) as a function of depth from the interface for both "pure" (dotted) and ~1M NaCl solutions (solid). The interface, 0 Å, is defined as the 50% dividing line of the density profile of water.

Like the experimental surface tensiometry, the density profiles show the minimal overall change in surface partitioning with the addition of salt. Immediately apparent is the strong surface activity of MGM (red). In both the pure and 1M NaCl simulations, MGM is largely centered at the interface with the minimal bulk concentration. In fact, the tail of this peak stretches past the aqueous surface and nearly to −5 Å, indicating that MGM is partitioning between the liquid and vapor phases, with a significant percentage of its population existing 1 Å–3 Å above the water interface. The changes to this

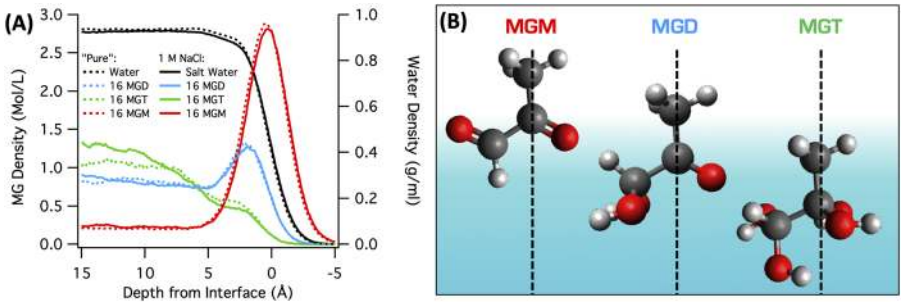

FIG. 7. Calculated MG density profiles and orientations: (a) density profiles from simulations of 16 MG (~1M) in pure water (dotted) and with 16 (~1M) NaCl (solid) for MGM (red), MGD (blue), MGT (green), and water (black). (b) Depiction of the general MGM, MGD, and MGT depth distributions and orientations of the C–CH_3 bond angle relative to the surface normal at the air–water interface calculated from molecular dynamics (MD) simulations of both neat-MG and MG–NaCl.

depth profile with the addition of salt are negligible, indicating that NaCl is not perturbing the solubility of MGM.

The same is true when comparing simulations of MGD solution in pure water to those with added NaCl. In each, MGD shows moderate bulk population at >5 Å but is significantly enhanced approaching the interface. MGT shows the largest variation, having a slightly greater preference for bulk solvation in the presence of salt. However, both the neat and salt simulations follow

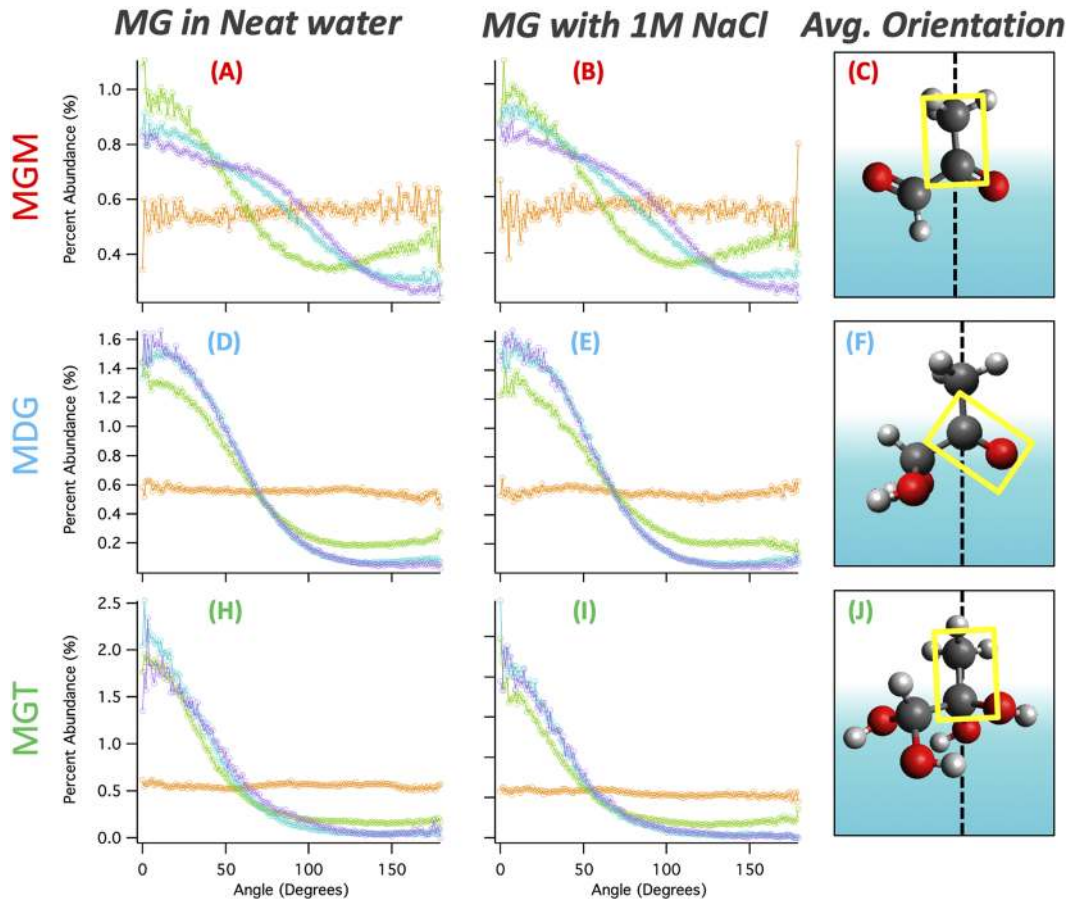

FIG. 8. Calculated MG depth dependent angle distributions: depth dependent angle distributions of the MG β-C–CH_3 bond angle with respect to the surface normal. Colored traces correspond to depth from the interface, describing the distribution for the bulk (10 Å, orange), subsurface (3 Å, green), surface (0 Å, blue), and supersurface (−1 Å, purple).

the same overall trend with the majority of the population in the bulk (>5 Å) and a sub-surface depletion approaching the interface. Overall, any changes observed in the presence of NaCl are too minimal to be considered significant.

B. MG orientation and angle distributions

The indications of a shift in hydration equilibrium discussed above merit a more careful analysis of each MG species in both neat and salt solutions. For each simulation, 1 Å slices of the box were analyzed to determine the average distributions of specific bond angles of MG (with respect to the surface normal) as a function of depth from the interface (Fig. 8 and Figs. S2–S4 of the supplementary material). The angle profiles reported here differ from those previously reported[15] as they have now been normalized by the sin(ø) and reported as percent abundance, allowing for a clearer determination of preferred orientation. It is important to note that these are not traditional surfactants and have highly dynamic surface behavior. Hence, these distributions are very much statistical averages, with the peak of the distribution signifying a preference toward that orientation, but with the molecules also continually moving and reorienting, as evidenced by the breadth of the distributions.

As with the density profiles, the addition of salt did not cause any significant change in orientation compared to the neat-MG results. In both neat-MG and Mg–NaCl simulations, MGM, MGD, and MGT each prefer to orient with their methyl groups pointing out of the interface between ~0° and 45° (centered at ~0°), as depicted in Fig. 7(b). From this, it is clear that the addition of salt does not by itself induce orientational changes in MG at the interface. MGM is the least ordered (broadest distribution), while MGT is the most constrained (narrowest distribution). We attribute this to MGT's enhanced hydrogen bonding ability maximizing its preferred orientation compared to the methyl orientation of MGM (and to a lesser extent, MGD), which is largely driven by hydrophobic forces.

Given MG's preference to hydrate and the density profiles discussed above, in experimental studies, any population of MGM will likely occur near or above the interface. As might be expected, the simulations show that the orientation of MGM becomes increasingly broad as it partitions further into the gas-phase. At 1 Å–2 Å above the interface, the preferred range of MGM methyl angle expands up to 90° beyond which the percent abundance sharply decreases. In this region, the decrease in hydrophobic forces on the methyl group allows a greater degree of freedom, while the proximity to the aqueous phase below still exerts repulsion that prevents the MGM from fully flipping its orientation. This indicates that the gas-phase MGM can take on some degree of order as it approaches the interface and is thus able to contribute to the VSF spectra. However, it still does not provide sufficient evidence to conclusively assign the ~2750 cm^{-1} mode seen in the VSF spectra of MGM.

V. CONCLUSIONS

To assess the effects of nonreactive salts on MG's surface behavior at the air–water interface, VSF measurements were performed on aqueous solutions of MG and NaCl. Our previous studies[15] on MG in neat water determined that MG is present at the interface as both the diol (MGD) and the tetrol (MGT) in a ratio of ~90:10, a greater monohydrate ratio than the 60:40 ratio reported in the bulk.[14,15] The current work builds on those studies and allows insight into how the system is perturbed by the presence of NaCl.

VSF spectra showed that the presence of NaCl significantly depresses the coordinated-OH stretching region relative to the MG–neat water system. The MG–NaCl system also demonstrated an increase in intensity for modes associated with MGD (and potentially MGM), while modes associated with MGT decreased in intensity.

The recent improvements to our picosecond laser system have also provided access to the bending region in the *sps* polarization, which was previously buried in the noise level. This has revealed spectral features and trends that were not observed during the original data collection of MG at the neat air–water interface. For example, in both polarization schemes, the feature assigned to water bending is now well defined when solvating MG in water. In combination, these new datasets confirm the assignment of the water bending mode and, thus, the presence of oriented interfacial water for both neat and salt solutions. The presence of C=C stretching modes in the VSF results also indicates the presence of larger oligomer species in the bending region, which requires further exploration.

The continued presence of a water mode in the bending region indicates that the observed changes in the stretching region are not merely due to increased surface partitioning and surface coverage from the salting out effects. Supporting this are surface pressure measurements, which show a relatively small increase in the presence of NaCl, <5 mN/m, as compared to the MG in the neat water system. Likewise, the computational results show a slight change in depth specific behavior or density relative to the pure MG–water system, in agreement with a minimal salting out effect. Analysis of

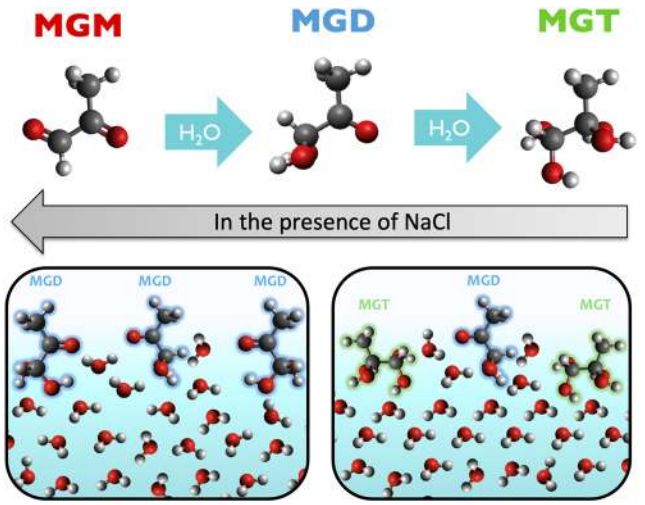

FIG. 9. Depiction of the potential explanation of a shift in MG hydration equilibrium underlying the enhancement of coordinated interfacial OH stretching modes in neat-MG and subsequent depletion with added salt: (bottom right) with four OH-groups, MGT enhances the OH-coordination at the interface. (Top) The addition of NaCl shifts the hydration equilibrium at the interface back toward MGD. (Bottom left) MGD has less OH-groups and does not solvate as neatly, disrupting the OH-coordination.

MG bond angles also demonstrates that orientational changes are minimal for all three MG hydration species. In combination, these results demonstrate that the local hydration equilibrium is shifted to even further favoring MGD (and potentially minimal amounts of MGM) at the air–water interface, with little to no MGT present at the interface, as depicted in Fig. 9.

This exploration of perturbations to MG by non-reactive NaCl salts will serve as a foundation for investigating the aqueous systems of MG in the presence of atmospherically relevant reactive salts, such as ammonium sulfate (AS).

SUPPLEMENTARY MATERIAL

See the supplementary material for a brief discussion of VSF water spectra; surface pressure values and error bars; tables of the values of DFT optimized structures, harmonic and anharmonic frequencies, and calculated VSF responses for each included conformer of MGM, MGD, and MGT; 1D MG ^{1}H and ^{13}C NMR and 2D HSQC NMR results; and ^{15}N NMR results of MG ruling out nitrogen contaminants.

DEDICATION

Dr. Sandra Greer's research has been crucial in establishing the generality of theories of phase transitions and in determining the exponents that describe critical behavior. Her experiments tested the view of reversible polymerizations as phase transitions. She has discovered new phenomena in the fractionations and conformations of polymers in solution. This paper is dedicated to Dr. Greer for her trail-blazing research and her many other contributions to science.

ACKNOWLEDGMENTS

This work was supported by the National Science Foundation under Grant Nos. CHE 1505891 and CHE 1051215. M.L.C. acknowledges financial support from ARCS Oregon Chapter.

DATA AVAILABILITY

The data that support the findings of this study are available from the corresponding author upon reasonable request.

REFERENCES

[1] B. Ervens and R. Volkamer, Atmos. Chem. Phys. **10**, 8219 (2010).
[2] B. Ervens, B. J. Turpin, and R. J. Weber, Atmos. Chem. Phys. **11**, 11069 (2011).
[3] N. Sareen *et al.*, Atmos. Chem. Phys. **10**, 997 (2010).
[4] B. Nozière, P. Dziedzic, and A. Córdova, Phys. Chem. Chem. Phys. **12**, 3864 (2010).
[5] D. O. De Haan *et al.*, Environ. Sci. Technol. **45**, 984 (2011).
[6] N. Sareen *et al.*, Proc. Natl. Acad. Sci. U. S. A. **110**, 2723 (2013).
[7] S. Gopalakrishnan *et al.*, J. Phys. Chem. B **109**, 8861 (2005).
[8] P. Jungwirth and D. J. Tobias, Chem. Rev. **106**, 1259 (2006).
[9] S. S. Petters *et al.*, ACS Earth Space Chem. **4**, 741 (2020).
[10] Y. Han *et al.*, Atmos. Environ. **126**, 290 (2016).
[11] K. Kawamura *et al.*, Atmos. Chem. Phys. **13**, 5369 (2013).
[12] K. Kawamura and S. Bikkina, Atmos. Res. **170**, 140 (2016).
[13] D. O. De Haan *et al.*, Environ. Sci. Technol. **43**, 8184 (2009).
[14] I. Nemet, D. Vikić-Topić, and L. Varga-Defterdarović, Bioorg. Chem. **32**, 560 (2004).
[15] S. N. Wren *et al.*, J. Phys. Chem. A **119**, 6391 (2015).
[16] K. W. Loeffler *et al.*, Environ. Sci. Technol. **40**, 6318 (2006).
[17] Y. Tan *et al.*, Atmos. Environ. **44**, 5218 (2010).
[18] F. Yasmeen *et al.*, Atmos. Chem. Phys. **10**, 3803 (2010).
[19] H. E. Krizner, D. O. De Haan, and J. Kua, J. Phys. Chem. A **113**, 6994 (2009).
[20] B. P. Gordon *et al.*, J. Phys. Chem. A **123**, 10609 (2019).
[21] A. N. Schwier *et al.*, Environ. Sci. Technol. **44**, 6174 (2010).
[22] E. M. Waxman *et al.*, Environ. Sci. Technol. **49**, 11500 (2015).
[23] R. J. Rapf *et al.*, J. Phys. Chem. A **121**, 8368 (2017).
[24] V. F. McNeill, Environ. Sci. Technol. **49**, 1237 (2015).
[25] E. M. Waxman *et al.*, Geophys. Res. Lett. **40**, 978, https://doi.org/10.1002/grl.50203 (2013).
[26] C. J. Kampf, R. Jakob, and T. Hoffmann, Atmos. Chem. Phys. **12**, 6323 (2012).
[27] S. Li *et al.*, Sci. Total Environ. **580**, 1155 (2017).
[28] C. D. Bain *et al.*, Langmuir **7**, 1563 (1991).
[29] K. B. Eisenthal, Chem. Rev. **96**, 1343 (1996).
[30] A. G. Lambert, P. B. Davies, and D. J. Neivandt, Appl. Spectrosc. Rev. **40**, 103 (2005).
[31] Y. R. Shen, J. Phys. Chem. C **116**, 15505 (2012).
[32] L. F. Scatena, M. G. Brown, and G. L. Richmond, Science **292**, 908 (2001).
[33] F. G. Moore, K. A. Becraft, and G. L. Richmond, Appl. Spectrosc. **56**, 1575 (2002).
[34] G. L. Richmond, Chem. Rev. **102**, 2693 (2002).
[35] P. G. Blower *et al.*, J. Phys. Chem. A **117**, 7887 (2013).
[36] N. A. Valley, E. J. Robertson, and G. L. Richmond, Langmuir **30**, 14226 (2014).
[37] N. A. Valley *et al.*, J. Phys. Chem. A **118**, 4778 (2014).
[38] L. E. McWilliams *et al.*, Phys. Chem. Chem. Phys. **17**, 21458 (2015).
[39] N. A. Valley and G. L. Richmond, J. Chem. Theory Comput. **11**, 4780 (2015).
[40] N. A. Valley and G. L. Richmond, J. Phys. Chem. C **120**, 14122 (2016).
[41] L. E. McWilliams *et al.*, J. Phys. Chem. A **121**, 7956 (2017).
[42] B. P. Gordon *et al.*, J. Phys. Chem. A **122**, 3837 (2018).
[43] B. K. Schabes, R. M. Altman, and G. L. Richmond, J. Phys. Chem. B **122**, 8582 (2018).
[44] B. K. Schabes, E. J. Hopkins, and G. L. Richmond, Langmuir **35**, 7268 (2019).
[45] Q. Du *et al.*, Phys. Rev. Lett. **70**, 2313 (1993).
[46] A. Morita and J. T. Hynes, Chem. Phys. **258**, 371 (2000).
[47] E. A. Raymond *et al.*, J. Phys. Chem. B **107**, 546 (2003).
[48] R. Lu *et al.*, J. Phys. Chem. B **108**, 7297 (2004).
[49] Y. R. Shen and V. Ostroverkhov, Chem. Rev. **106**, 1140 (2006).
[50] C. S. Tian and Y. R. Shen, Chem. Phys. Lett. **470**, 1 (2009).
[51] R.-r. Feng *et al.*, J. Phys. Chem. A **115**, 6015 (2011).
[52] D. Verreault, W. Hua, and H. C. Allen, J. Phys. Chem. Lett. **3**, 3012 (2012).
[53] M. Vinaykin and A. V. Benderskii, J. Phys. Chem. Lett. **3**, 3348 (2012).
[54] Y. Nagata *et al.*, J. Phys. Chem. Lett. **4**, 1872 (2013).
[55] Y. Ni and J. L. Skinner, J. Chem. Phys. **143**, 014502 (2015).
[56] G. R. Medders and F. Paesani, J. Am. Chem. Soc. **138**, 3912 (2016).
[57] A. Kundu *et al.*, J. Phys. Chem. Lett. **7**, 2597 (2016).
[58] F. Perakis *et al.*, Chem. Rev. **116**, 7590 (2016).
[59] R. Khatib *et al.*, J. Phys. Chem. C **120**, 18665 (2016).
[60] C. Dutta and A. V. Benderskii, J. Phys. Chem. Lett. **8**, 801 (2017).
[61] S. Pezzotti, D. R. Galimberti, and M.-P. Gaigeot, J. Phys. Chem. Lett. **8**, 3133 (2017).
[62] Y. Suzuki, Y. Nojima, and S. Yamaguchi, J. Phys. Chem. Lett. **8**, 1396 (2017).
[63] F. Tang *et al.*, J. Chem. Theory Comput. **14**, 357 (2018).
[64] S. Woutersen, U. Emmerichs, and H. J. Bakker, Science **278**, 658 (1997).
[65] P. R. Monson *et al.*, Chem. Phys. Lett. **28**, 312 (1974).
[66] L. Chieffo *et al.*, Chem. Phys. **341**, 71 (2007).
[67] S. Knop, J. Lindner, and P. Vöhringer, Z. Phys. Chem. **225**, 913 (2011).

[68]J. A. Donarski, D. P. T. Roberts, and A. J. Charlton, Anal. Methods **2**, 1479 (2010).
[69]J. H. Kroll *et al.*, J. Geophys. Res.: Atmos. **110**, 23207, https://doi.org/10.1029/2005JD006004 (2005).
[70]C. J. Kampf *et al.*, Environ. Sci. Technol. **47**, 4236 (2013).
[71]D. A. Case *et al.*, AMBER 12, University of California, San Francisco, 2012.
[72]L. Martínez *et al.*, J. Comput. Chem. **30**, 2157 (2009).
[73]M. J. Frisch *et al.*, Gaussian, 09, 2009,
[74]M. K. Maron *et al.*, Chem. Phys. Lett. **513**, 184 (2011).
[75]M. C. Larsen and V. Vaida, J. Phys. Chem. A **116**, 5840 (2012).
[76]E. C. Griffith *et al.*, Proc. Natl. Acad. Sci. U. S. A. **110**, 11714 (2013).
[77]A. E. Reed Harris *et al.*, J. Phys. Chem. A **118**, 8505 (2014).
[78]R. J. Perkins *et al.*, J. Phys. Chem. A **120**, 10096 (2016).
[79]A. E. Reed Harris *et al.*, J. Phys. Chem. A **120**, 10123 (2016).
[80]A. E. Reed Harris *et al.*, J. Phys. Chem. A **121**, 3327 (2017).
[81]R. J. Rapf *et al.*, J. Phys. Chem. A **121**, 4272 (2017).
[82]R. J. Rapf *et al.*, J. Am. Chem. Soc. **139**, 6946 (2017).
[83]A. E. Reed Harris *et al.*, J. Phys. Chem. A **121**, 8348 (2017).
[84]R. J. Rapf *et al.*, ACS Cent. Sci. **4**, 624 (2018).
[85]Y. Fang *et al.*, J. Phys. Chem. A **123**, 983 (2019).
[86]M. R. Alves *et al.*, J. Phys. Chem. A **123**, 7661 (2019).
[87]G. K. Glushonok *et al.*, Russ. J. Gen. Chem. **73**, 1027 (2003).